Supporting information

A selective electrochemical chiral interface based on carboxymethyl-β-cyclodextrin/Pd@Au nanoparticles/3D reduced graphene oxide nanocomposite for tyrosine enantiomers recognition

Qingfang Niu[1], Pengyue Jin[2], Yu Huang[1], Lifang Fan[1], Caihong Zhang[1], Cheng Yang[2]*, Chuan Dong [1], Wenting Liang[1]*, Shaomin Shuang [1]*

[1]   *Institute of Environmental Sciences, Department of Chemistry, Shanxi University, Taiyuan 030006, China.*

[2]   *College of Chemistry, Sichuan University, 29 Wangjiang Road, Chengdu 610064, China*
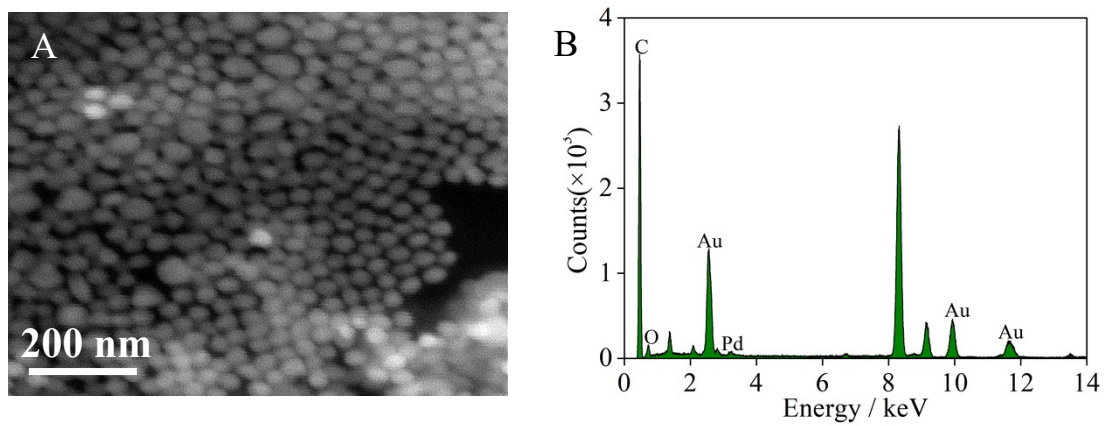
Fig. S1 SEM image (A) and EDS spectrum (B) of Pd@Au NPs.
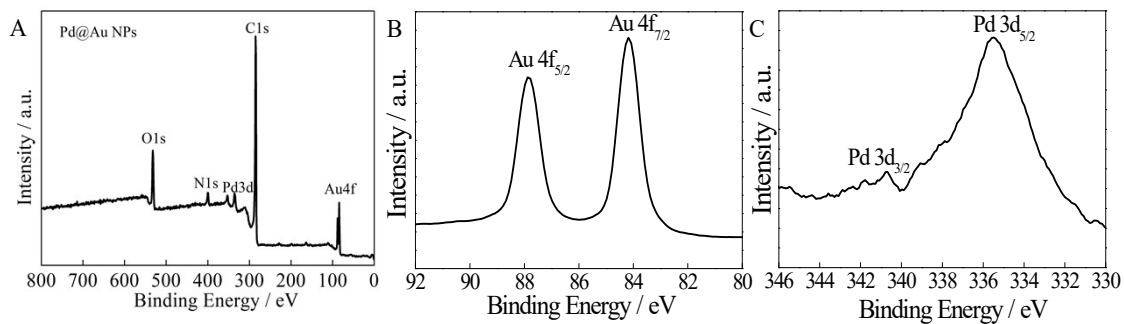
Fig. S2 XPS spectra of Pd@Au NPs.
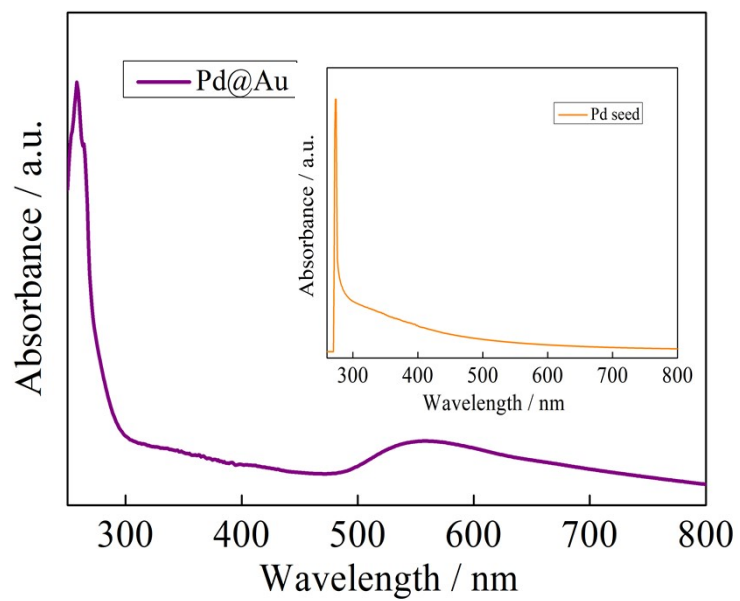
Fig. S3 UV-vis absorption of Pd@Au NPs. The insert is UV-vis absorption of Pd seeds.
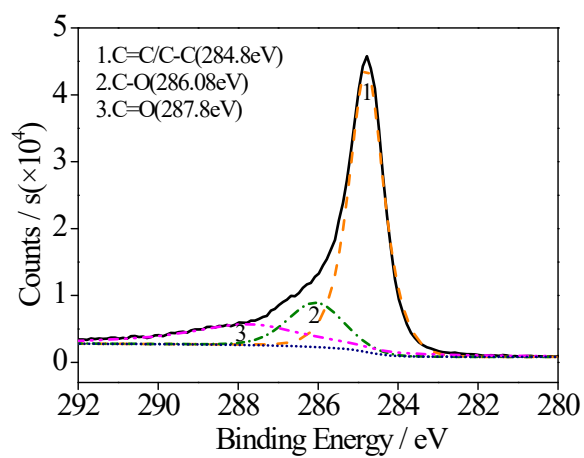
Fig. S4 XPS C 1s spectrogram for 3D-rGO/Pd@Au.
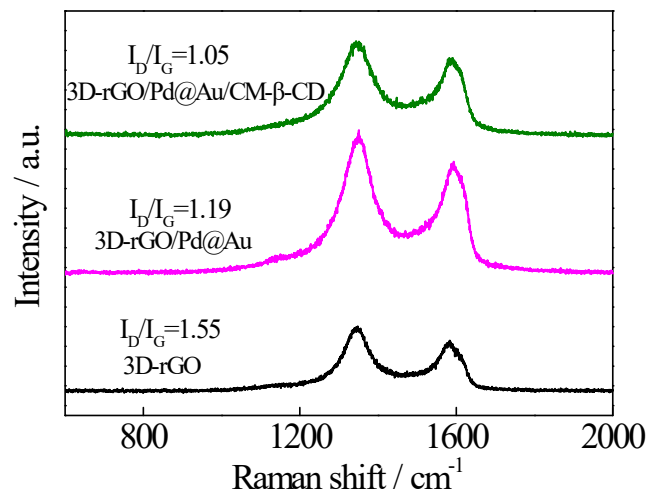
Fig. S5 Raman spectra for 3D-rGO, 3D-rGO/Pd@Au and 3D-rGO/Pd@Au/ CM-β-CD.
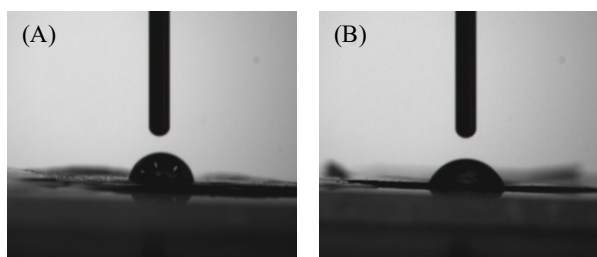
Fig. S6 Contact-angle photographs of 3D-rGO/Pd@Au (a) and 3D-rGO/Pd@Au/CM-β-CD (b) modified substrates.

The contact angles for water of 3D-rGO/Pd@Au and 3D-rGO/Pd@Au/CM-β-CD film were measured to be 84.6° and 71°, respectively (Fig. S6a and 6b). Among two material films, 3D-rGO/Pd@Au displays relatively strong hydrophobic interface with the higher contact angle due to the reduction of the hydrophilic oxygen-containing groups from GO. The smaller contact angle of the 3D-rGO/Pd@Au/CM-β-CD film relative to 3D-rGO/Pd@Au manifestes its weaker hydrophobic, which is explained by the hydrophilic groups of the water-soluble CM-β-CD molecules.
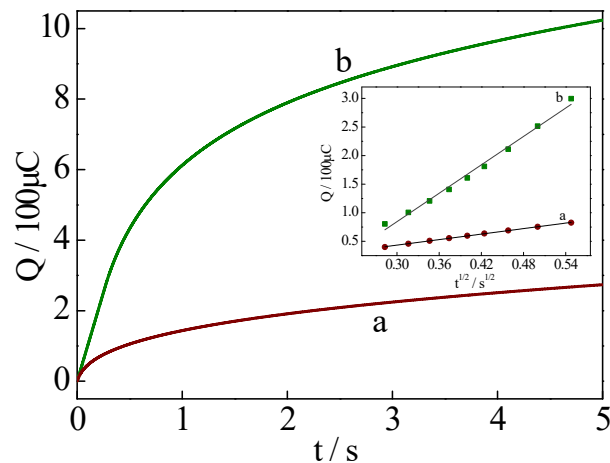
Fig. S7 Plot of Q-t curves of GCE (a) and 3D-rGO/Pd@Au/CM-β-CD/GCE (b) in 0.1 mM $K_3[Fe(CN)_6]$ containing 1.0 M KCl. Inset: Plot of Q-$t^{1/2}$ curves on GCE (a) and 3D-rGO/Pd@Au/CM-β-CD/GCE (b).

In Fig. S7, the effective surface areas, A of bare GCE and 3D-rGO/Pd@Au/CM-β-CD/GCE were calculated according to the following equation:

$$Q = 2nFAcD^{1/2}t^{1/2}/\pi^{1/2} + Q_{dl} + Q_{ads}$$

where Q is the capacitive charge of the measured electrode surface at t, n is the number of electron transfer, F ($C \cdot mol^{-1}$) is the Faraday constant, A (cm^2) stands for the surface area of the electrode, c ($mol \cdot cm^{-3}$) represents the concentration of substrate, D ($cm^2 \cdot s^{-1}$) is the diffusion coefficient, Q_{dl} is the double layer charge and Q_{ads} is the adsorption charge. It turns out that A is 0.1071 cm^2 for bare GCE and 0.5523 cm^2 for 3D-rGO/Pd@Au/CM-β-CD/GCE.

Optimization of recognition conditions
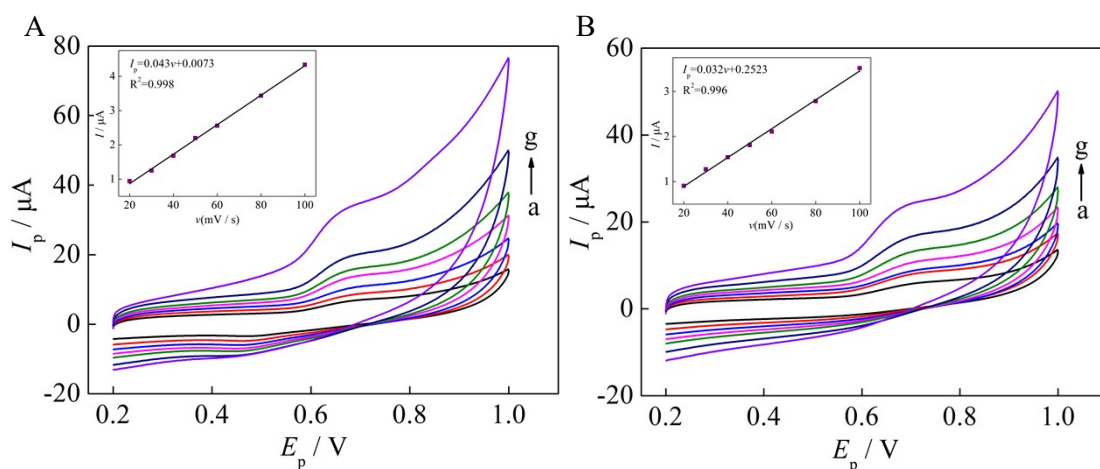
Fig. S8 CVs of 3D-rGO/Pd@Au/CM-β-CD/GCE for (A) L-Tyr and (B) D-Tyr (1.0 mM, containing 0.1 M PB, pH 7.0) at different scan rate (20, 30, 40, 50, 60, 80 and 100 mV s^{-1}, scanned from 0.2 to 1.0 V; the insert curve of I_p (oxidation peak current) versus scan rate (v) of L-Tyr and D-Tyr at 3D-rGO/Pd@Au/CM-β-CD/GCE.
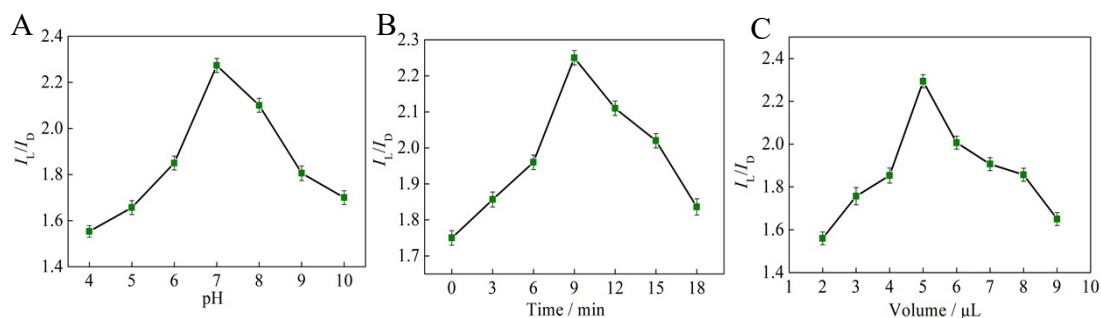
Fig. S9 Influence of pH (A), the volume (B) and the accumulation time (C) on the enantiorecognition efficiency (I_L/I_D) of 3D-rGO/Pd@Au/CM-β-CD toward Tyr isomers.
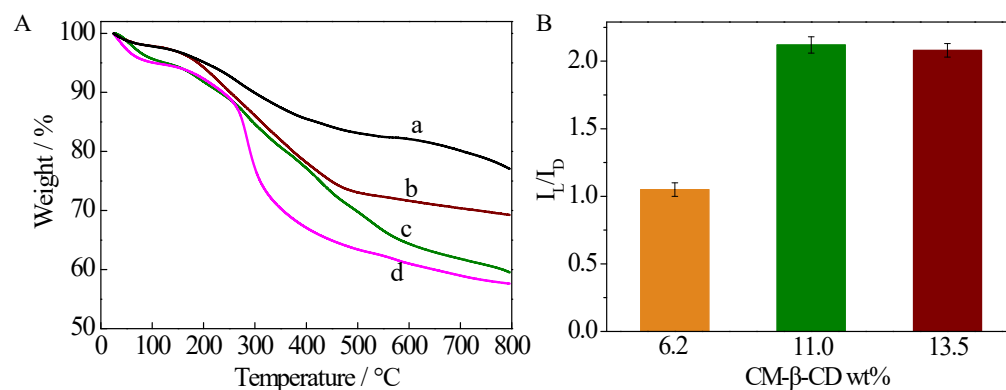
Fig. S10 (A) TGA of 3D-rGO/Pd@Au (a) and 3D-rGO/Pd@Au/CM-β-CD containing different amounts of CM-β-CD (b-d); (B) The CM-β-CD amounts of 3D-rGO/Pd@Au/CM-β-CD influence on the recognition efficiency of 3D-rGO/Pd@Au/CM-β-CD/GCE toward Tyr isomers.

Influence of sweep speed

The effects of scanning rate on 3D-rGO/Pd@Au/CM-β-CD/GCE for L-Tyr and D-Tyr were studied to resolve the surface characteristics of the developed sensor. As shown in Fig. S8, the electrochemical redox of Tyr enantiomers at 3D-rGO/Pd@Au/CM-β-CD/GCE is irreversible. The oxidation peak current of L- or D-Tyr linearly increased with an enhanced scan rate (v) in the range of 10 to 100 mV/s. The linear equations of L-Tyr and D-Tyr are $I_p= 0.043v+0.0073$ ($R^2=0.998$) and $I_p= 0.032v+0.2523$ ($R^2=0.996$), respectively. The results indicated that the electrochemical sensor of L/D-Tyr at 3D-rGO/Pd@Au/CM-β-CD/GCE is an adsorption-control process [1]. As depicted in the insert curve of Fig. S8A and S8B, it can be seen that the slope of the linear regression equation of L-Tyr is greater than that of D-Tyr, which might be ascribed to the fact that the intermolecular interactions between the 3D-rGO/Pd@Au/CM-β-CD based interface and L-Tyr are relatively higher, resulting in higher peak currents. These results are also consistent with those of DPV (Fig. 4D).

Influence of the pH

It should be pointed out that the pH values of the Tyr solutions greatly affect the electrochemical behavior of the designed 3D-rGO/Pd@Au/CM-β-CD/GCE in the oxidation process of Tyr, which turned out to be different chiral discrimination. As Fig. S9A shown, it is found that the peek current ratio of Try isomers (I_L/I_D) first increased and then decreased in the pH range from 4.0 to 10.0, and the maximum of I_L/I_D occurs at pH 7.0, which is considered as the optimum pH for the experiment.

Influence of the accumulation time

As shown in Fig. S9B, the accumulation time is important factor for enantiorecognition efficiency. The peak current ratio of I_L/I_D increases rapidly with the increase of incubation time in the beginning, and achieves to the maximum at 9 min, meaning that the adsorption equilibriums reached. Even so, it is observed that the I_L/I_D value decreases continuously with further increasing time. Thus, 9 min is selected as the optimum accumulation time to obtain the highest recognition efficiency of Tyr isomers in the present work.

Influence of the amount of 3D-rGO/Pd@Au/CM-β-CD

The modification amount of 3D-rGO/Pd@Au/CM-β-CD dispersion also affects the

enantiorecognition efficiency of tyrosine isomers. By controlling the modification amount of 3D-rGO/Pd@Au/CM-β-CD dispersion, the thickness of the sensor layer can be adjusted to change the electron transfer rate. It can be clearly observed that the oxidation peak has a maximum current value when the modification amount is 5 μL (Fig. S9C). Therefore, 5 μL is selected as a suitable volume drop of 3D-rGO/Pd@Au/CM-β-CD and coated on the surface of GCE for detection.

Optimizing the amount of CM-β-CD carried by 3D-rGO/Pd@Au

The recognition ability of the 3D-rGO/Pd@Au/CM-β-CD chiral platform was simultaneously conjugated to the peculiarity of 3D-rGO/Pd@Au with excellent electrical conductivity and CM-β-CD as chiral host for enantiorecognition. Therefore, it is noteworthy that the grafting amount of CM-β-CD molecules onto the 3D-rGO/Pd@Au has a significant influence on the electrochemical discrimination of Tyr enantiomers. Three kinds of prepared 3D-rGO/Pd@Au/CM-β-CD materials have been characterized by TGA, and the amounts of CM-β-CD carried by 3D-rGO/Pd@Au were 6.2 wt%, 11.0 wt% and 13.5 wt%, respectively (Fig. S10A). Furthermore, the recognition efficiency (I_L/I_D) of these three materials has been explored and recorded by DPV approach. As shown in Fig. S10B, the 3D-rGO/Pd@Au containing 11.0 wt% CM-β-CD exhibits more prominent enantiorecognition ability than the 6.2 wt% 3D-rGO/Pd@Au/CM-β-CD and similar with the 13.5 wt% 3D-rGO/Pd@Au/CM-β-CD. The results illustrate that the appropriate amount of CM-β-CD is beneficial for Tyr enantiomer recognition. Hence, 11.0 wt% of CM-β-CD is selected as the optimum amount to obtain the good recognition efficiency of Tyr isomers in the present work.

References

1. Arvine A, Mahosenaho M, Pinteala M, et al. Electrochemical oxidation of p-nitrophenol using graphene-modified electrodes, and a comparison to the performance of MWNT-based electrodes. Microchim Acta, 2011, 174(3-4): 337-343.
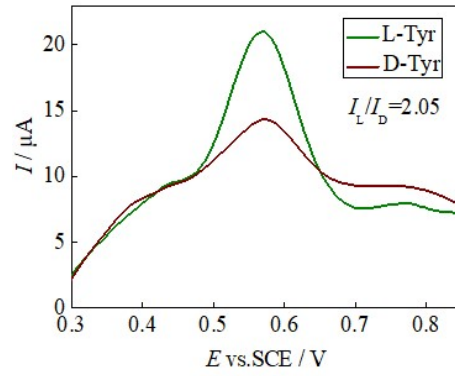
Fig. S11 Differential pulse voltammograms of 1 mM L-Tyr and D-Tyr at 3D-rGO/CM-β-CD/GCE in 0.1 M PBS solution (pH 7.0).
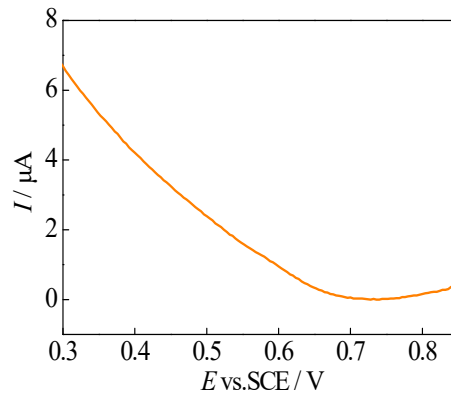
Fig.S12 Differential pulse voltammograms of 3D-rGO/Pd@Au/CM-β-CD/GCE in 0.1 M PBS (pH 7.0).
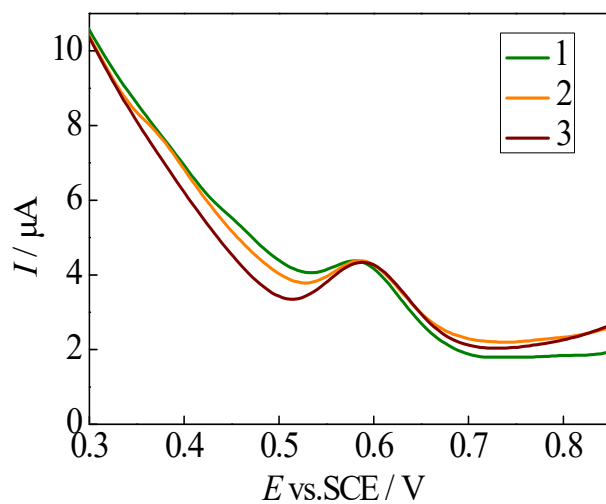
Fig. S13 DPV plots of 3D-rGO/Pd@Au/CM-β-CD/GCE in pH 7.0 PBS containing 200 μM L-Tyr for reproducibility by using the three different batches of materials.
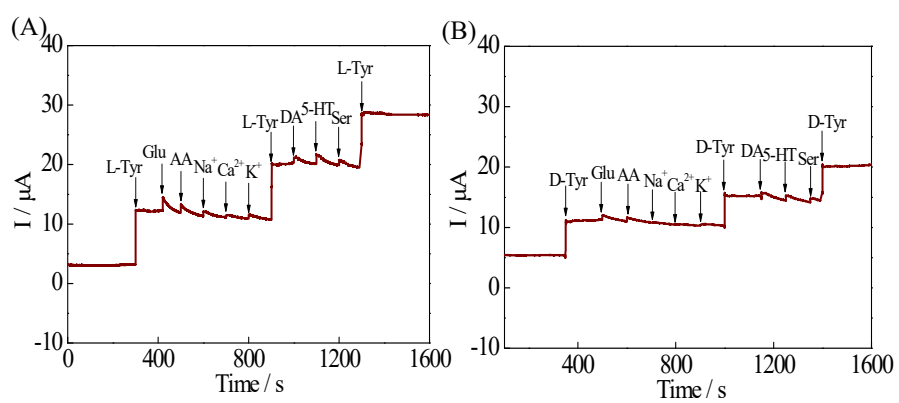
Fig. S14 Amperometric responses of the 3D-rGO/Pd@Au/CM-β-CD/GCE for the addition of 100 μM L-Tyr (A) and 100 μM D-Tyr (B) with 300 μM Glu, AA, Na$^+$, Ca^{2+}, K$^+$, DA, 5-HT, Ser in 0.1 mol/L PBS (pH = 7.0).

Table S1 Comparison of different chiral sensors in the recognition efficiency of Tyr enantiomers.

Modified Electrode	Method	Recognition difference (ΔI, μA)	Linear range (mol L^{-1})	LOD(mol L^{-1})	Ref.
MPC-SCD/GCE	DPV	$\Delta I = (I_D - I_L) = 1.12$	$1 \times 10^{-6} - 5 \times 10^{-4}$(L/D)	2.6×10^{-7}(L) 2×10^{-7}(D)	[41]
rGO-CHMF/GCE/	DPV	$I_L/I_D = 1.58$	$1 \times 10^{-7} - 1 \times 10^{-4}$(L/D)	7.8×10^{-8}(L) 8.3×10^{-8}(D)	[42]
L-Cys-Au/Fe$_3$O$_4$/MGCE	SWV	$I_L/I_D = 1.85$	$1 \times 10^{-6} - 1.25 \times 10^{-3}$(L/D)	1.2×10^{-8}(L) 8.4×10^{-8}(D)	[43]
SS-CS/GCE	SWV	$I_L/I_D = 1.38$	$1 \times 10^{-5} - 1 \times 10^{-3}$(L/D)	3.5×10^{-7}(L) 4.2×10^{-7}(D)	[44]
[(SA)Zn(II)(L/D-Tyr)]/GCE	CV	$I_L/I_D = 1.24$	-	-	[45]
GSH-Cu/Pt/GCE	DPV	$I_L/I_D = 5.11$	-	-	[46]
CS-GalN/GCE	SWV	$I_L/I_D = 1.70$	$1 \times 10^{-5} - 1 \times 10^{-4}$(L/D)	6.5×10^{-7}(L) 8.6×10^{-7}(D)	[47]
SGO-NH$_2$-β-CD/BPNSs/GCE	SWV	$I_D/I_L = 1.94$	$1 \times 10^{-5} - 1 \times 10^{-3}$(L/D)	1.74×10^{-6}(L) 1.02×10^{-7}(D)	[48]
CS-SA/GCE	SWV	$I_L/I_D = 1.63$	-	-	[49]
α-Fe$_2$O@Co$_3$O$_4$-NRGO/CCE	SDLSV	-	$1 \times 10^{-8} - 1 \times 10^{-5}$(L/D)	8×10^{-9}(L/D)	[50]
3D-rGO/Pd@Au/CM-β-CD/GCE	DPV	$I_L/I_D = 2.12$	$8 \times 10^{-7} - 1.3 \times 10^{-4}$(L/D)	5.2×10^{-8}(L) 9.6×10^{-8}(D)	This work
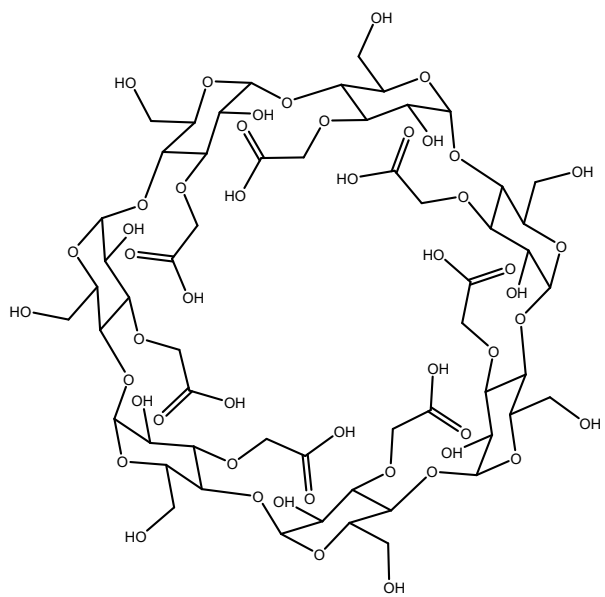
Fig. S15 The structure of CM-β-CD.
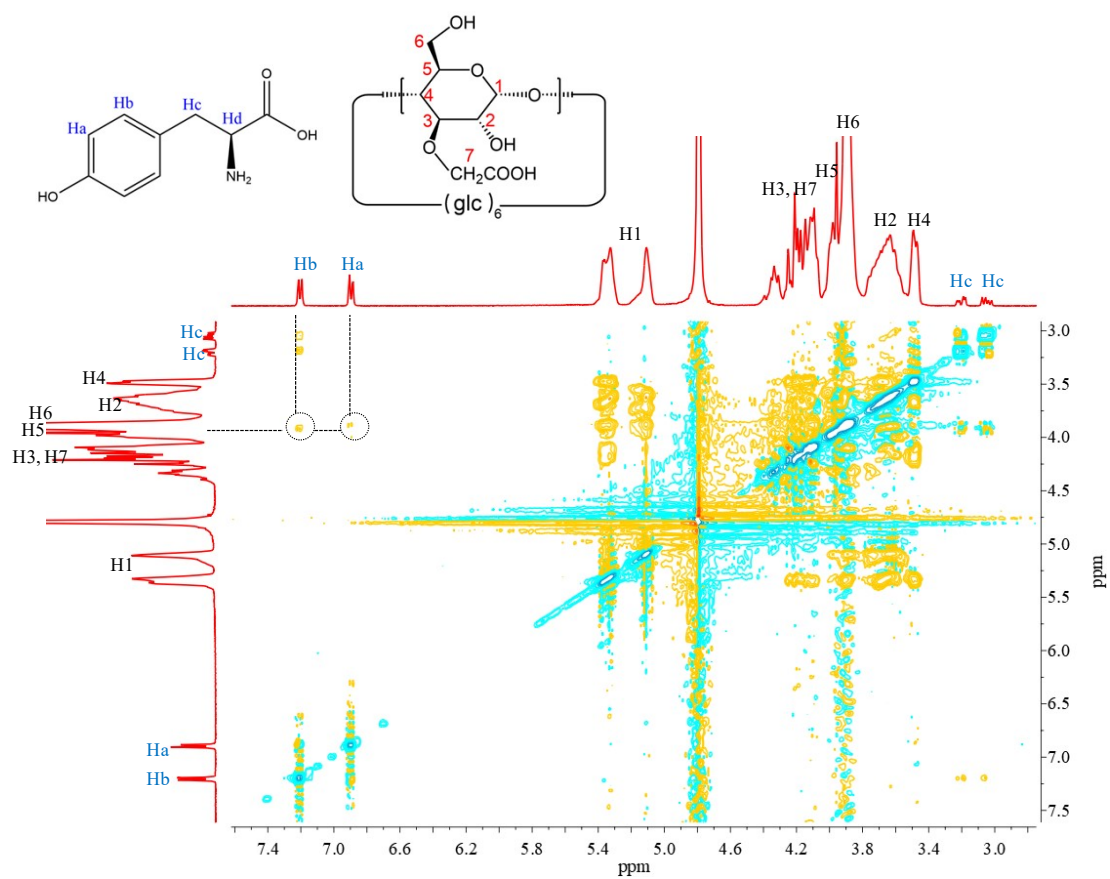
Fig. S16 ROESY spectrum of an equimolar mixture of L-Tyr (2.5 mM) and CM-β-CD (2.5 mM) in D₂O
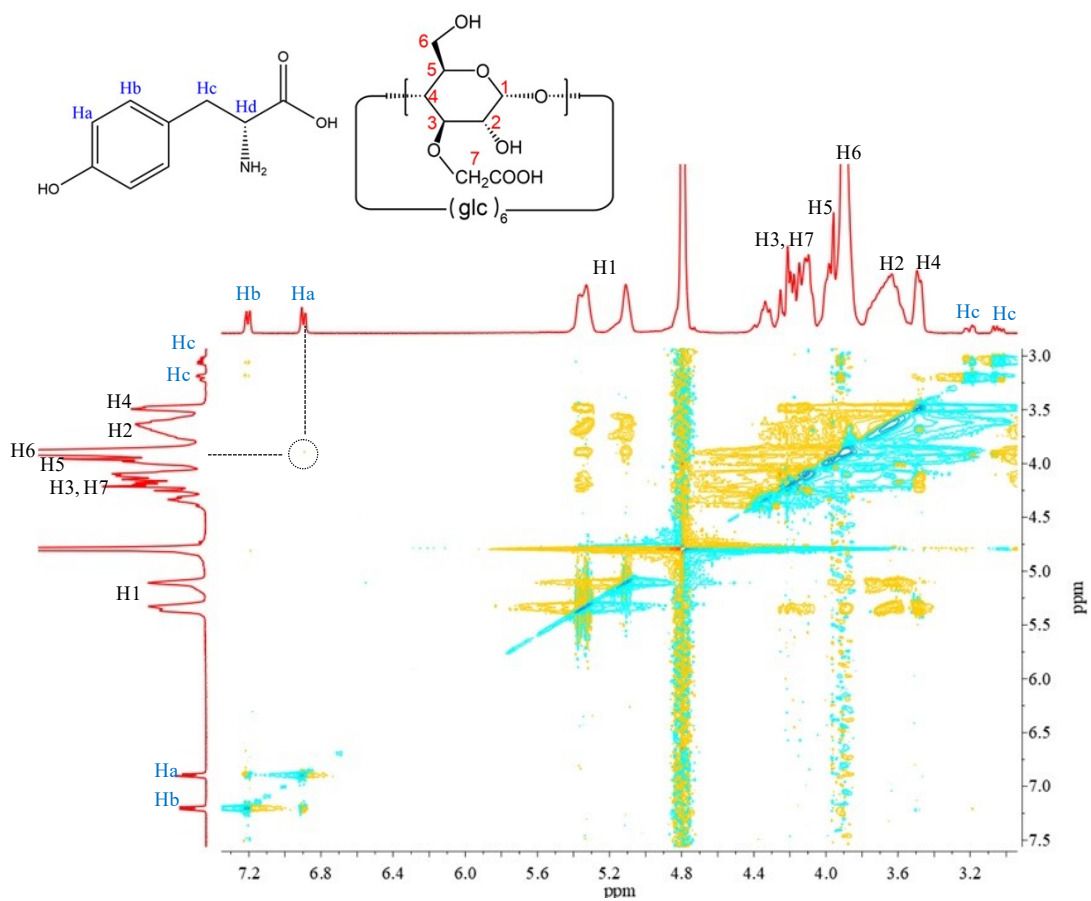
Fig. S17 ROESY spectrum of an equimolar mixture of D-Tyr (2.5 mM) and CM-β-CD (2.5 mM) in D_2O

Enantiomeric excess (% ee) is an invaluable parameter for the estimation of the success of chemical processes occurring in these fifields since it defifines the purity of non-racemic mixtures of chiral compounds. It is usually defifined as:

$$\% \text{ ee} = \frac{[R]_t - [S]_t}{[R]_t + [S]_t} \times 100 \%$$

where $[R]_t$ and $[S]_t$ are the respective total analytical concentrations of the (R)- and (S)-enantiomers of analyte (guest).
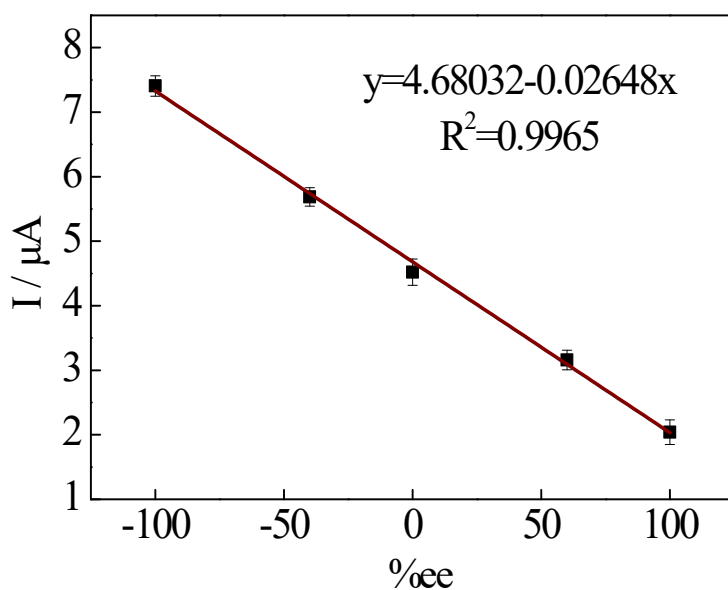
Fig. S18 Linear relationship between I_A and % ee in the mixture of Tyr isomers (1 mM).